CLASSIFICATION:

Biological Sciences / Genetics

TITLE:

Sex Chromosome Dosage Effects on Gene Expression in Humans

AUTHORS AND AUTHOR AFFILIATIONS:

Armin Raznahan*[1], Neelroop Parikshak[2], Vijayendran Chandran[3], Jonathan Blumenthal[1], Liv Clasen[1], Aaron Alexander-Bloch[1], Andrew Zinn[4], Danny Wangsa[5], Jasen Wise[6], Declan Murphy[7], Patrick Bolton[7], Thomas Ried[5], Judith Ross[8], Jay Giedd[9], Daniel Geschwind[2]

1. *Developmental Neurogenomics Unit, National Institute of Mental Health, NIH, Bethesda, MD, USA*
2. *Neurogenetics Program, Department of Neurology and Center for Autism Research and Treatment, Semel Institute, David Geffen School of Medicine, University of California Los Angeles, Los Angeles, CA, USA*
3. *Department of Pediatrics, School of Medicine, University of Florida, Gainesville, FL 32610-0296, USA*
4. *McDermott Center for Human Growth and Development and Department of Internal Medicine, University of Texas Southwestern Medical School, TX, USA*
5. *Genetics Branch, Center for Cancer Research, National Cancer Institute, NIH, Bethesda, MD, USA*
6. *Qiagen, Frederick, MD, USA*
7. *Institute of Psychiatry, Psychology and Neuroscience, King's College London, University of London, UK*
8. *Department of Pediatrics, Thomas Jefferson University, Philadelphia, PA, USA*
9. *Department of Psychiatry, UC San Diego, La Jolla, CA, USA*

CORRESPONDING AUTHOR:

Armin Raznahan MD PhD, Developmental Genomics Unit, Rm 4D18, Building 10, 10 Center Drive, National Institute of Mental Health, NIH, Bethesda, MD, USA, T: 3014357927, E: raznahana@mail.nih.gov

KEYWORDS:

Sex chromosomes; X-chromosome; Y-chromosome; dosage compensation; X-inactivation; sex differences; Turner syndrome: Klinefelter syndrome: ZFX

ABSTRACT:

A fundamental question in the biology of sex-differences has eluded direct study in humans: how does sex chromosome dosage (SCD) shape genome function? To address this, we developed a systematic map of SCD effects on gene function by analyzing genome-wide expression data in humans with diverse sex chromosome aneuploidies (XO, XXX, XXY, XYY, XXYY). For sex chromosomes, we demonstrate a pattern of obligate dosage sensitivity amongst evolutionarily preserved X-Y homologs, and update prevailing theoretical models for SCD compensation by detecting X-linked genes whose expression increases with decreasing X- and/or Y-chromosome dosage. We further show that SCD-sensitive sex chromosome genes regulate specific co-expression networks of SCD-sensitive autosomal genes with critical cellular functions and a demonstrable potential to mediate previously documented SCD effects on disease. Our findings detail wide-ranging effects of SCD on genome function with implications for human phenotypic variation.

SIGNIFICANCE STATEMENT:

Sex chromosome dosage (SCD) effects on human gene expression are central to the biology of sex differences and sex chromosome aneuploidy syndromes, but challenging to study given the co-segregation of SCD and gonadal status. We address this obstacle by systematically modelling SCD effects on genome-wide expression data from a large and rare cohort of individuals with diverse SCDs (XO, XX, XXX, XXXX, XY, XXY, XYY, XXYY, XXXXY). Our findings update current models of sex chromosome biology by (i) pinpointing a core set of X- and Y-linked genes with “obligate” SCD sensitivity, (ii) discovering several non-canonical modes of X-chromosome dosage compensation, and (iii) dissecting complex regulatory effects of X-chromosome dosage on large autosomal gene networks with key roles in cellular functioning.

INTRODUCTION

Disparity in SCD is fundamental to the biological definition of sex throughout much of the animal kingdom. In almost all eutherian mammals, females carry two X-chromosomes, while males carry an X- and a Y-chromosome: presence of the Y-linked SRY gene determines a testicular gonadal phenotype, while its absence allows development of ovaries (1). Sexual differentiation of the gonads leads to hormonal sex-differences that have traditionally been considered the major proximal cause for extra-gonadal phenotypic sex-differences. However, diverse studies, including recent work in transgenic mice that uncouple Y-chromosome and gonadal status, have revealed direct SCD effects on several sex-biased metabolic, immune and neurological phenotypes (2).

These findings - together with reports of widespread transcriptomic differences between pre-implantation XY and XX embryos (3, 4) - suggest that SCD has gene regulatory effects independently of gonadal status. However, genome-wide consequences of SCD remain poorly understood, especially in humans, where experimental dissociation of SCD and gonadal status is not possible. Understanding these regulatory effects is critical for clarifying the biological underpinnings of phenotypic sex-differences, and the clinical features of sex chromosome aneuploidy (5) [SCA, e.g. Turner (XO) and Klinefelter (XXY) syndrome], which can both manifest as altered risk for several common autoimmune and neurodevelopmental disorders (e.g. systemic lupus erythematosus and autism spectrum disorders) (6, 7). Here, we explore the

genome wide consequences of SCD through comparative transcriptomic analyses amongst humans across a range of dosages including typical XX and XY karyotypes, as well as several rare SCA syndromes associated with 1, 3, 4 or 5 copies of the sex chromosomes. We harness these diverse karyotypes to dissect the architecture of dosage compensation amongst sex chromosome genes, and to systematically map the regulatory effects of SCD on autosomal gene expression in humans.

We examined gene expression profiles in a total of 470 lymphoblastoid cell lines (LCLs), from (i) a core sample of 68 participants (12 XO, 10 XX, 9 XXX, 10 XY, 8 XXY, 10 XYY, 9 XXYY) yielding for each sample genome-wide expression data for 19,984 autosomal and 894 sex-chromosome genes using the Illumina oligonucleotide Beadarray platform (**Methods**), and (ii) an independent set of validation/replication samples from 402 participants (4 XO, 146 XX, 22 XXX, 145 XY, 33 XXY, 16 XYY, 17 XXYY, 8 XXXY, 10 XXXXY) with quantitative reverse transcription polymerase chain reaction (qPCR) measures of expression for genes of interest identified in our core sample (**Table S1, Methods**).

RESULTS

Extreme Dosage Sensitivity of Evolutionarily Preserved X-Y Gametologs

To first verify our study design as a tool for probing SCD effects on gene expression, and to identify core SCD-sensitive genes, we screened all 20,878 genes in our microarray dataset to define which, if any, genes showed a persistent pattern of significant differential expression (DE) across all unique

141 pairwise group contrasts involving a disparity in either X- or Y-chromosome
142 dosage (n=15 and n=16 contrasts respectively, **Fig. 1a**). Disparities in X-
143 chromosome dosage were always accompanied by statistically significant DE in
144 4 genes, which were all X-linked: *XIST* (the orchestrator of X-inactivation) and 3
145 other known genes known to escape X-chromosome inactivation (*PUDP*,
146 *KDM6A*, *EIF1AX*) (8). Similarly, disparities in Y-chromosome dosage always led
147 to statistically-significant DE in 6 genes, which were all Y-linked: *CYorf15B*,
148 *DDX3Y*, *TMSB4Y*, *USP9Y*, *UTY,* and *ZFY*. Observed expression profiles for
149 these 10 genes perfectly segregated all microarray samples by karyotype group
150 (**Fig. 1b**), and could be robustly replicated and extended using available qPCR
151 data for 5/5 of these genes in the independent sample of 402 LCLs from
152 participants with varying SCD (**Fig. S1, Methods**).

153 Strikingly, 8 of the 10 genes showing obligatory SCD sensitivity (excepting
154 XIST and PUPD) are members of a class of 16 sex-linked genes with homologs
155 on both the X and Y chromosomes (i.e. 16 X-Y gene pairs, henceforth
156 gametologs) (9) that are distinguished from other sex-linked genes by (i) their
157 selective preservation in multiple species across ~300 million years of sex
158 chromosome evolution to prevent male-female dosage disparity, (ii) the breadth
159 of their tissue expression from both sex chromosomes; and (iii) their key
160 regulatory roles in transcription and translation (9, 10) (**Fig. 1c**). Broadening our
161 analysis to all 14 X-Y gametolog pairs present in our microarray data found that
162 these genes as a group exhibit a heightened degree of SCD-sensitivity that
163 distinguishes them from other sex-linked genes (**Fig. 1d, Methods**). These

164 findings provide direct evidence that the evolutionary maintenance, broad tissue
165 expressivity and enriched regulatory functions of X-Y gametologs (10) are indeed
166 accompanied by a distinctive pattern of dosage sensitivity, which firmly
167 establishes these genes as candidate regulators of SCD effects on wider
168 genome function.
169
170 **Figure 1 (next page). Consistent Gene Expression Changes with Altered Sex Chromosome**
171 **Dosage. a)** Cross table showing all unique pairwise SCD group contrasts within our microarray
172 dataset, color coded for their involvement of changes in X- and Y-chromosome count. **b)** Two-
173 dimensional expression heat-map for the 10 genes showing differential expression across all
174 contrasts that involve disparity in X or Y-chromosome count. Column colors encode SCD group
175 membership for each sample. Rows detail gene expression across all SCD samples as a log 2
176 fold change relative to the mean expression in XY males. **c)** Table providing Gene ID, location,
177 function and homolog annotations for the 10 genes that showed obligate SCD sensitivity. Eight
178 genes in this set are members of X-Y gametolog gene pairs. **d)** Density plots showing observed
179 mean SCD sensitivity of the 14 gametolog genes in our study (red line), vs. null distribution (black
180 line) of mean SCD sensitivity for 10,000 randomly sampled sets of non-gametolog sex-linked
181 genes of equal size. Results are provided separately for X- and Y-chromosomes. For both
182 chromosomes, the mean SCD sensitivity of the gametolog gene set is greater is than that of all
183 10k permuted gene sets.
184

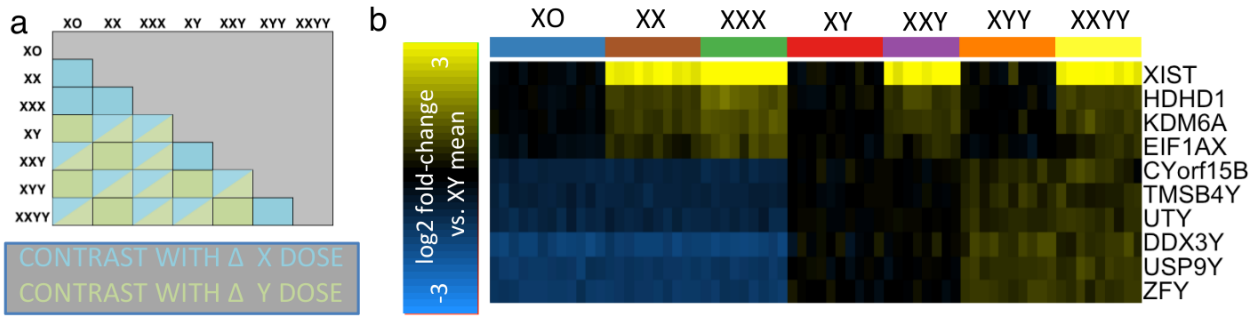

c

Gene_Name (Alias)	Entrez_ID	Chromosome	Probe_Start	Probe_End	Functions	Gametolog_Name (Alias)	Functions
PUDP (HDHD1)	8226	X	6967201	6967250	encodes protein of unknown biological function	-	-
KDM6A (UTX)	7403	X	44970808	44970857	catalyzes the demethylation of tri/dimethylated histone H3	UTY	protein-protein interactions
XIST	7503	X	73040921	73040970	essential for initiation and spread of X inactivation	-	-
EIF1AX	1964	X	20150300	20150326	essential translation initiation factor	EIF1AY	translation initiation
Gene_Name (Alias)	**Entrez_ID**	**Chromosome**	**Probe_Start**	**Probe_End**	**Functions**	**Gametolog_Name (Alias)**	**Functions**
ZFY	7544	Y	2849596	2849645	transcription factor	ZFX	transcription factor
USP9Y	8287	Y	14971985	14972034	ubiquination	USP9X	ubiquination
DDX3Y	8653	Y	15032184	15032233	RNA and ATP binding, hydrolysis	DDX3X	RNA helicase, transcriptional regulation and translation
UTY	7404	Y	15360382	15360431	protein-protein interactions	KDM6A (UTX)	catalyzes the demethylation of tri/dimethylated histone H3
TMSB4Y (TB4Y)	9087	Y	15817595	15817644	uncharacterized	TMSB4X (TB4X)	actin polymerization, cell proliferation/differentiation
TXLNGY (CYorf15B)	84663	Y	21765838	21765887	pseudogene	TXLNG	transcriptional regulation, intracellular trafficking

d

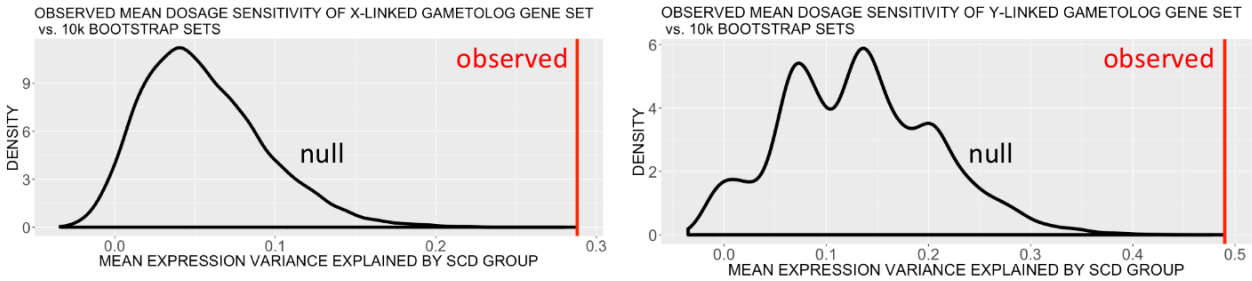

Observed Sex Chromosome Dosage Effects on X- and Y-chromosome Genes Modify Current Models of Dosage Compensation

We next harnessed our study design to test the canonical ("Four Class") model for SCD compensation, which defines four mutually-exclusive classes of

192 sex chromosome genes that would be predicted to have differing responses to
193 changing SCD(11): (i) pseudoautosomal region (PAR) genes, (ii) Y-linked genes,
194 (iii) X-linked genes that undergo X-chromosome inactivation (XCI), and (iv) X-
195 linked genes that "escape" XCI (XCIE). Under the Four Class Model, PAR genes
196 would be predicted to increase their expression with increases in X- or Y-
197 chromosome count, whereas expression of Y-linked genes would increase
198 linearly with mounting Y-chromosome count. Due to the non-binary nature of
199 gene silencing with XCI (12), theorized SCD effects on expression of XCI and
200 XCIE genes represent extreme ends of an X-chromosome dosage sensitivity
201 continuum: an X-linked genes that undergoes full silencing with XCI would show
202 no expression change with changes in X-chromosome dosage, whereas an X-
203 linked gene that undergoes complete escape from X-chromosome inactivation
204 would show a linear increase in expression with increasing X-chromosome count.
205 To test this canonical "Four Class Model" we considered all sex
206 chromosome genes and performed unsupervised *k*-means clustering of genes by
207 their mean expression in each of the 7 karyotype groups represented in our
208 microarray dataset, and compared this empirically-defined grouping with that
209 given *a priori* by the Four Class Model (**Methods**). *k*-means clustering
210 distinguished 5 reproducible (color-coded) clusters of SCD-sensitive sex-
211 chromosome genes that overlapped strongly with gene groups predicted by the
212 Four Class Model, from a large left-over cluster of 773 genes with low or
213 undetectable expression levels in most samples (median detection rate of 4/68
214 samples), and no significant SCD sensitivity (**Table S2, Fig. 2a,b, Fig. S2a,b**).

215 The 5 SCD-sensitive groups of sex chromosome genes detected by k-
216 means were highly reproducible over k-means analyses across 1000 bootstrap
217 draws from our sample pool (**Fig. S2b**), and consisted of: an Orange cluster of
218 PAR genes, a Pink cluster of Y-linked genes (especially enriched for Y
219 gametologs, odds ratio=5213, $p=1.3*10^{-15}$), a Green cluster enriched for known
220 XCIE genes (especially X gametologs, odds ratio=335, $p=3.4*10^{-11}$), and a
221 Yellow cluster enriched for known XCI genes. The X-linked gene responsible for
222 initiating X-inactivation - XIST - fell into its own Purple "cluster" (**Fig. 2b**). For all
223 but the Orange cluster of PAR genes, observed patterns of gene-cluster dosage
224 sensitivity across karyotype groups deviated from those predicted by the Four
225 Class Model (**Fig. 2c**).

226 Mean Expression for the Pink cluster of Y-linked genes increased in a
227 stepwise fashion with Y-chromosome dosage, but deviated from the Four Class
228 Model prediction by showing a sub-linear relationship with Y-chromosome count
229 – indicting that these Y-linked genes may be subject to active dosage
230 compensation. Fold-changes observed by microarray for 3/3 of these Y-linked
231 genes were highly correlated across group contrasts with fold-changes observed
232 between karyotype groups by qPCR in an independent sample of 402
233 participants with varying SCD (**Methods, Fig. S2d).**

234 Observed expression profiles the Yellow and Green clusters of X-linked
235 genes also deviated from predictions of the Four Class Model predictions (**Table**
236 **S2, Fig. 2c,d**). Linear models for X- and Y-chromosome dosage effects on
237 expression (**Methods**) indicated that the XCI-enriched Yellow cluster was highly

238 sensitive to SCD (F=47.7, $p<2.2*10^{-16}$), and that the expression of this cluster
239 was significantly *inversely* related to X-chromosome dosage at the level of both
240 mean cluster expression (coefficient for linear effect of X-chromosome count on
241 expression = -0.12, $p=3.8*10^{-15}$) and the individual expression profile of 60/66
242 genes within the cluster ($p<0.05$ for negative linear effect of X count on
243 expression). This observation suggests that increasing X copy number may not
244 solely involve silencing of these genes from the additional inactive X-
245 chromosome, but a further repression of their expression from the single active
246 X-chromosome.

247 Remarkably, expression of the XCI gene cluster was also significantly
248 decreased by presence of a Y-chromosome, at the level of both mean cluster
249 expression (coefficient for linear effect of Y-chromosome count on expression = -
250 0.09, $p= 1.4*10^{-14}$) and expression profiles of 48/66 individual cluster genes
251 ($p<0.05$ for negative linear effect of Y count on expression). The Green XCIE
252 cluster manifested an inverted version of this effect whereby increases in Y
253 chromosome dosage were associated with increased gene expression ($p<$
254 $6.2*10^{-11}$ for mean cluster expression and $p<0.05$ for 23/39 cluster genes) -
255 providing the first evidence that Y-chromosome status can influence the
256 expression level of X-linked genes independently of circulating gonadal factors.
257 Mean expression of Green XCIE cluster genes also scaled sub-linearly with X-
258 chromosome dosage. For both Green and Yellow clusters, we established that
259 observed patterns of dosage sensitivity held when analysis was restricted to X-
260 linked genes with only high confidence annotations for XCIE and XCI status

261 (respectively) (**Fig 2d**) – suggesting that observed expression profiles was
262 unlikely to be explained by misclassification of X-linked genes by XCI status. To
263 further probe the sublinear relationship between XCIE Green cluster expression
264 and X-chromosome dosage, we integrated our findings with those of a recently-
265 published (13) survey of allelic expression imbalance analyses from female
266 LCLs with skewed X-inactivation (**Text S1, Fig. S2**). This analysis revealed that
267 the magnitude of observed sub-linear relationships between Green cluster gene
268 expression values and X-chromosome dosage is consistent with independent
269 measurements of incomplete of escape from XCI (12, 13).

270 To determine the reproducibility and convergent validity of the unexpected
271 modes of dosage sensitivity observed for XCI (reduced expression with
272 increasing X- and Y-chromosome dosage) and XCIE (increased expression with
273 increasing Y-chromosome dosage) clusters, we first confirmed that the distinct
274 expression profiles for these two clusters were reproducible at the level of
275 individual genes and samples. Indeed, unsupervised clustering of microarray
276 samples based on expression of XCI and XCIE cluster genes relative to XX
277 controls distinguished three broad karyotype groups: females with one X-
278 chromosome (XO), males with one X-chromosome (XY, XYY), and individuals
279 with extra X-chromosome (XXX, XXY, XXYY) (**Fig. 2e**). We were also able to
280 validate our data-driven discovery of XCI and XCIE gene clusters against
281 independently generated X-chromosome annotations (**Fig. 2f**), which detail 3
282 distinct genomic predictors of inactivation status for X-linked genes. Specifically,
283 XCI cluster genes were relatively enriched (and XCIE cluster genes relatively

284 impoverished) for (i) having lost a Y-chromosome homolog during evolution (14)
285 (X^2 = 10.9, p=0.01), (ii) being located in older evolutionary strata of the X-
286 chromosome (15) (X^2 = 22.6, p=0.007), and (iii) bearing heterochromatic markers
287 (16) (X^2 = 18.35, p=0.0004).

288 Finally, qPCR assays in LCLs from an independent sample of 402
289 participants with varying SCD validated the fold changes observed in microarray
290 data for 5/6 of the most SCD-sensitive XCIE and XCI cluster genes (**Methods,**
291 **Fig. S2e**). To independently extend these observations, we measured gene
292 expression by qPCR in novel karyotype groups not represented in our microarray
293 dataset (XXXY, XXXXY, **Methods**) and were able to confirm reduction in
294 expression with greater X-chromosome dosage for 2 of 3 XCI cluster genes (**Fig**
295 **S2f**, *NGFRAP1*, *CXorf57*), and Y-chromosome dosage effects upon expression
296 for 5 of 6 X-linked genes from XCI and XCIE clusters (**Fig S2g**, downregulation:
297 *NGFRAP1*, *CXorf57* | up-regulation: *PIM2*, *PRKX).* Taken together, these
298 findings update the canonical Four Class Model of SCD compensation for
299 specific Y-linked and X-linked genes, and expand the list of X-linked genes
300 capable of mediating wider phenotypic consequences of SCD variation.
301
302
303
304
305
306
307

308 **Figure 2 (next page). Data-Driven Partitioning of Sex Chromosome Genes by Dosage**
309 **Sensitivity. a)** 2D Multidimensional scaling (MDS) plot of sex chromosome genes by their mean
310 expression profiles (+/- 95% confidence intervals) across all 7 SCD groups. Genes are coded by
311 both Four Class Model and k-means cluster grouping. Note that MDS2 arranges X-linked genes
312 along the established gradient of X-linked dosage sensitivity that ranges from extreme XCIE
313 (XIST), to full XCI. **b)** Cross table showing enrichment of k-means clusters (rows) for Four Class
314 Model gene groups. Lower-bounds for enrichment odds-ratios are given where mean enrichment
315 = ∞. **c)** Dot and line plots showing observed and predicted mean expression values for each k-
316 means gene cluster across karyotype groups. **d)** Close-up of observed (solid, color-coded) vs.
317 predicted (dashed, gray) mean (+/- 95% confidence intervals) expression profiles of Green and
318 Yellow gene clusters. Observed expression profiles still counter predictions when analysis is
319 restricted to core genes in each cluster with XCIE/XCI status that has been confirmed across
320 three independent reports (Balaton et al). **e)** Heatmap showing normalized (vs. XX mean)
321 expression of dosage sensitive genes in the XCIE and XCI k-means groups (rows, color-coded
322 green and yellow respectively), for each sample (columns, color coded by SCD group). **f)** Pie-
323 charts showing how genes within XCIE and XCI-enriched k-means clusters (green and yellow
324 columns respectively), display mirrored over/under-representation for three genomic features of
325 X-linked gene that have been linked to XCEI in prior research (i) persistence of a surviving Y-
326 linked homolog, (ii) location of the gene within "younger" evolutionary strata of the X-
327 chromosome, and (iii) presence of euchromatic rather than heterochromatic epigenetic markers.
328
329

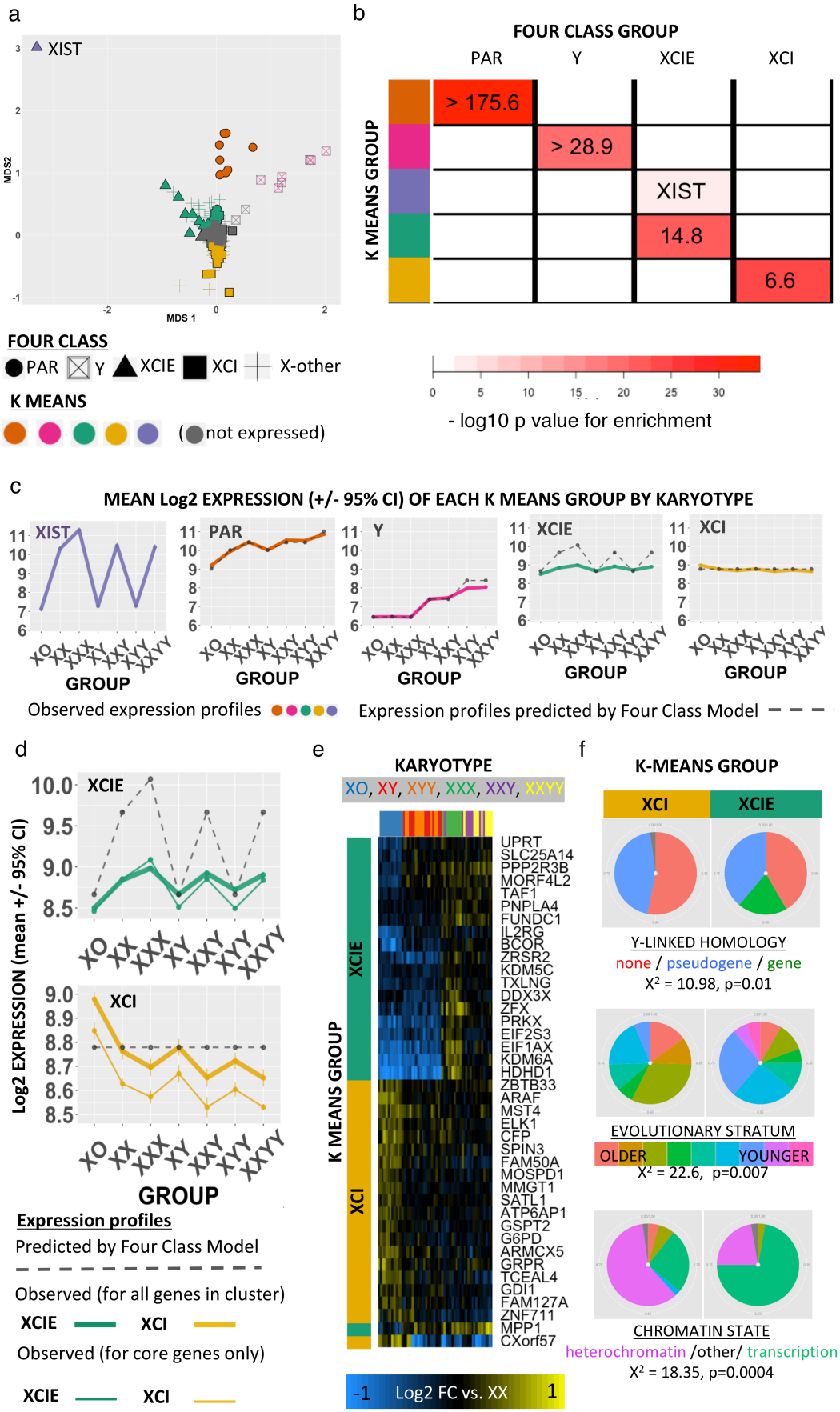
a
XIST
MDS2
MDS 1
FOUR CLASS
PAR
Y
XCIE
XCI
X-other
K MEANS
(not expressed)
b
FOUR CLASS GROUP
PAR
Y
XCIE
XCI
K MEANS GROUP
> 175.6
> 28.9
XIST
14.8
6.6
- log10 p value for enrichment
c
MEAN Log2 EXPRESSION (+/- 95% CI) OF EACH K MEANS GROUP BY KARYOTYPE
XIST
PAR
Y
XCIE
XCI
GROUP
Observed expression profiles
Expression profiles predicted by Four Class Model
d
XCIE
XCI
Log2 EXPRESSION (mean +/- 95% CI)
GROUP
Expression profiles
Predicted by Four Class Model
Observed (for all genes in cluster)
XCIE
XCI
Observed (for core genes only)
XCIE
XCI
e
KARYOTYPE
XO, XY, XYY, XXX, XXY, XXYY
K MEANS GROUP
XCIE
XCI
UPRT
SLC25A14
PPP2R3B
MORF4L2
TAF1
PNPLA4
FUNDC1
IL2RG
BCOR
ZRSR2
KDM5C
TXLNG
DDX3X
ZFX
PRKX
EIF2S3
EIF1AX
KDM6A
HDHD1
ZBTB33
ARAF
MST4
ELK1
CFP
SPIN3
FAM50A
MOSPD1
MMGT1
SATL1
ATP6AP1
GSPT2
G6PD
ARMCX5
GRPR
TCEAL4
GDI1
FAM127A
ZNF711
MPP1
CXorf57
-1
Log2 FC vs. XX
1
f
K-MEANS GROUP
XCI
XCIE
Y-LINKED HOMOLOGY
none / pseudogene / gene
X² = 10.98, p=0.01
EVOLUTIONARY STRATUM
OLDER
YOUNGER
X² = 22.6, p=0.007
CHROMATIN STATE
heterochromatin /other/ transcription
X² = 18.35, p=0.0004

330

331 **Context-Specific Disruption of Autosomal Expression by Sex Chromosome**
332 **Aneuploidy**

333 We next leveraged the diverse SCAs represented in our study to assess
334 how SCD variation shapes expression on a genome-wide scale. By counting the
335 total number of differentially expressed genes (DEGs, **Methods**) in each SCA
336 group relative to its respective euploidic control (i.e XO and XXX compared with
337 XX; XXY, XYY, XXYY compared with XY), we detected order of magnitude
338 differences in DEG count amongst SCAs across a range of log2 fold change
339 (log2FC) cut-offs (**Fig. 3a,b**). We observed an order of magnitude increase in
340 DEG count with X-chromosome supernumeracy in males vs. females, which
341 although previously un-described, is congruent with the more severe phenotypic
342 consequences of X-supernumeracy in males vs. females (17). Overall, increasing
343 the dosage of the sex chromosome associated with the sex of an individual (i.e.
344 X in females and Y in males) had a far smaller effect than other types of SCD
345 changes. Moreover, the ~20 DEGs seen in XXX contrasted with >2000 DEGs in
346 XO – revealing a profoundly asymmetric impact of X-chromosome loss vs. gain
347 on the transcriptome of female LCLs, which echoes the asymmetric phenotypic
348 severity of X-chromosome loss (Turner) vs. gain (XXX) syndromes in females (6).

349 To clarify the relative contribution of sex chromosome vs. autosomal
350 genes to observed DEG counts with changes in SCD, we calculated the
351 proportion of DEGs in every SCD group (comparing SCAs to their "gonadal
352 controls", and XY males to XX females) that fell within each of four distinct
353 genomic regions: autosomal, PAR, Y-linked and X-linked (**Fig. 3c**). Autosomal

genes accounted for >75% of all DEGs in females with X-monosomy (XO) and males with X-supernumeracy (XXY, XXYY), but <30% DEGs in all other SCD groups (**Methods**). These results reveal that SCD changes vary widely in their capacity to disrupt genome function, and demonstrate that differential involvement of autosomal genes is central to this variation. Moreover, associated SCA differences in overall DEG count broadly recapitulate SCA differences in phenotypic severity.

Figure 3 (next page). Genome-wide Effects of Sex Chromosome Dosage Variation. a-b) Table **a** and corresponding line-plot **b** showing number of genes with significant differential expression (after FDR correction with q<0.05) in different SCD contrasts at varying |log2 fold change| cut-offs. Note the order-of-magnitude differences between the number of Differentially Expressed Genes (DEGs) in XO ("removal of X from female") vs. XXY and XXYY ("addition of X to male") vs. XYY and XXX ("addition of Y and X to male and female, respectively"). A |log2 fold change| threshold of 0.26 (~20% change in expression) was applied to categorically define differential expression in other analyses, by identifying the log2 fold change threshold increase causing the greatest drop in DEG count for each karyotype group, and then averaging this value across karyotype groups. **c)** Dot-and-line plot showing the proportion of DEGs in each karyotype group that fell within different regions of the genome. The proportion of all genes in the genome within each genomic region is shown for comparison. All SCD groups showed non-random DEG distribution relative to the genome (p<2*10^-16), but DEG distributions differed significantly between SCD groups (p<2*10^-16). XO, XXX and XXYY are distinguished from all other SCDs examined by the large fraction of their overall DEG count that comes from autosomal genes.

a

DOSAGE CHANGE	CONTRAST	LOG2 FOLD CHANGE CUT-OFF			
		0.26	0.5	1	2
Loss of X in female	XO vs. XX	2204	469	50	7
Addition of X in male	XXY vs. XY	268	85	13	1
	XXYY vs. XY	266	93	9	2
Addition of Y in male	XYY vs. XY	34	15	0	0
Addition of X in female	XXX vs. XX	28	7	3	1

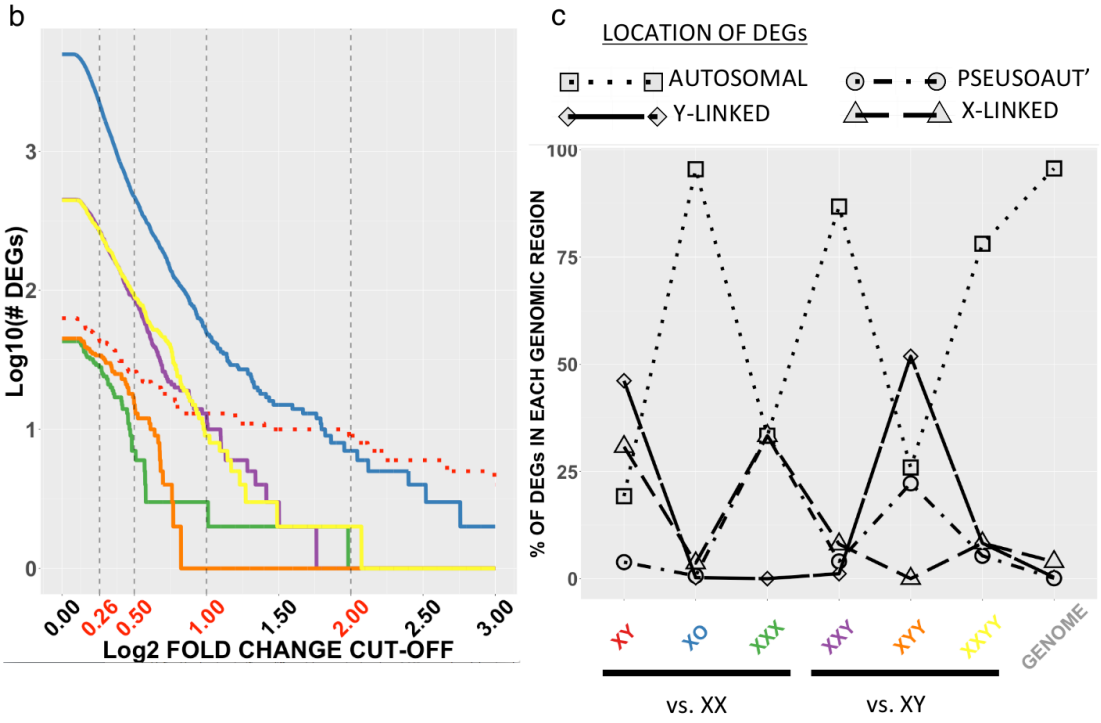

Sex Chromosome Dosage Regulates Large-Scale Gene Co-expression Networks

To provide a more comprehensive systems-level perspective on the impact of SCD on genome-wide expression patterns, we leveraged Weighted Gene Co-expression Network Analysis (18) (WGCNA, **Methods**). This analytic approach uses the correlational architecture of gene expression across a set of samples to detect sets (modules) of co-expressed genes. Using WGCNA, we identified 18 independent gene co-expression modules in our dataset (**Table S3**).

390 We established that these modules were not artifacts of co-differential expression
391 of genes between groups by demonstrating their robustness to removal of all
392 group effects on gene expression by regression (**Fig. S3a**), and after specific
393 exclusion of XO samples (**Fig. S3b**) given the extreme pattern of DE in this
394 karyotype (**Fig. 3b**). We focused further analysis on modules meeting 2
395 independent statistical criteria after correction for multiple comparisons: (i)
396 significant omnibus effect of SCD group on expression, (ii) significant enrichment
397 for one or more gene ontology (GO) process/function terms (**Methods, Table S3,**
398 **Fig. 4a-b**). These steps defined 8 functionally coherent and SCD-sensitive
399 modules (Blue, Brown, Green, Purple, Red, Salmon, Tan and Turquoise).
400 Notably, the SCD effects we observed on genome wide expression patterns
401 appeared to be specific to shifts in sex chromosome gene dosage, as application
402 of our analytic workflow to publically available genome-wide Illumina beadarray
403 expression data from LCLs in patients with trisomy 21 (Down syndrome)
404 revealed a highly dissimilar profile of genome-wide expression change to that
405 observed in sex chromosome trisomies (**Methods, Fig. 4c, Table S4**).

406 To specify SCA effects on module expression, we compared all
407 aneuploidy groups to their respective "gonadal controls" (**Fig. 4d**). Statistically
408 significant differences in modular eigengene expression were seen in XO, XXY
409 and XXYY groups - consistent with these karyotypes causing larger total DE
410 gene counts than other SCD variations (**Fig. 3a**). The largest shifts in module
411 expression were seen in XO, and included robust up-regulation of protein
412 trafficking (Turquoise), metabolism of non-coding RNA and mitochondrial ATP

413 synthesis (Brown), and programmed cell death (Tan) modules, alongside down-
414 regulation of cell cycle progression, DNA replication/chromatin organization
415 (Blue, Salmon), glycolysis (Purple) and responses to endoplasmic reticular stress
416 (Green) modules. Module DE in those with supernumerary X chromosomes on
417 an XY background, XXY and XXYY, involved "mirroring" of some XO effects –
418 i.e. *down-regulation* of protein trafficking (Turquoise) and *up-regulation* of cell-
419 cycle progression (Blue) modules – plus a more karyotype-specific up-regulation
420 of immune response pathways (Red).

421 The distinctive up-regulation of immune-system genes in samples of
422 lymphoid tissue from males carrying a supernumerary X-chromosome carries
423 potential clinical relevance for one of the best-established clinical phenotypes in
424 XXY and XXYY syndromes: a strongly (up to 18-fold) elevated risk for
425 autoimmune disorders (ADs) such as Systemic Lupus Erythmatosus, Sjogren
426 Syndrome, and Diabetes Mellitus (7). In further support of this interpretation, we
427 found the Red module to be significantly enriched (p=0.01 by Fisher's Test, and
428 p=0.01 by gene set permutation) for a set of known AD risks compiled from
429 multiple large-scale Genome Wide Association Studies (GWAS**, Methods**). The
430 two GWAS implicated AD risk genes showing strongest connectivity within the
431 Red module and up-regulation in males bearing an extra X-chromosome were
432 *CLECL1* and *ELF1* – indicating that these two genes should be prioritized for
433 further study in mechanisms of risk for heightened autoimmunity in XXY and
434 XXYY males. Collectively, these results represent the first systems-level
435 characterization of SCD effects on genome function, and provide convergent

436 evidence that increased risk for AD risk in XXY and XXYY syndrome may be
437 arise due to an up-regulation of immune pathways by supernumerary X-
438 chromosomes in male lymphoid cells.

439 To test for evidence of coordination between the changes in sex-
440 chromosome genes imparted by SCD (**Fig. 2**), and the genome-wide
441 transcriptomic variations detected through WGCNA (**Fig. 4a**), we asked if any
442 SCD-sensitive gene co-expression modules were enriched for one or more of the
443 5 SCD-sensitive clusters of sex chromosome genes (i.e. "PAR", "Y-linked",
444 "XCIE", "XCI" and the gene XIST). Four WGCNA modules - all composed of
445 >95% autosomal genes - showed such enrichment (**Fig. 4e**): The Turquoise and
446 Brown modules were enriched for XCI cluster genes, whereas the Green and
447 Blue modules were enriched for XCIE cluster genes. The Blue module was
448 unique for its additional enrichment in PAR genes, and its inclusion of XIST. We
449 generated network visualizations to more closely examine SCD-sensitive genes
450 and gene co-expression relationships within each of these four sex-chromosome
451 enriched WGCNA modules (**Fig. 4f** Blue and **Fig. S3c-e** for others**, Methods)**.
452 The Blue module network highlights XIST, select PAR genes (*SLC25A6*,
453 *SFRS17A*) and multiple X-linked genes from X-Y gametolog pairs (*EIF1AX*,
454 *KDM6A* (*UTX*), *ZFX*, *PRKX*) for their high SCD-sensitivity, and shows that these
455 genes are closely co-expressed with multiple SCD-sensitive autosomal genes
456 including *ZWINT*, *TERF2IP* and *CDKN2AIP*.

457 Our detection of highly-organized co-expression relationships between
458 SCD sensitive sex-linked and autosomal genes hints at specific regulatory effects

459 of dosage sensitive sex chromosome genes in mediating the genome-wide
460 effects of SCD variation. To test this, and elucidate potential regulatory
461 mechanisms, we performed an unbiased transcription factor binding site (TFBS)
462 enrichment analysis of genes within Blue, Green, Turquoise and Brown WGCNA
463 modules (**Methods**). This analysis converged on a single TF - ZFX, encoded by
464 the X-linked member of an X-Y gametolog pair – as the only SCD sensitive TF
465 showing significant TFBS enrichment in one or more modules. Remarkably, the
466 gene *ZFX* was itself part of the Blue module, and ZFX binding sites were not only
467 enriched amongst Blue and Green module genes (increased in expression with
468 increasing X-chromosome dose), but also amongst Brown module genes that are
469 downregulated as X-chromosome dose increases (**Fig. 4g)**. To directly test if
470 changes in ZFX expression are sufficient to modify expression of Blue, Green or
471 Brown modules genes in immortalized lymphocytes, we harnessed existing
472 gene-expression data from murine T-lymphoblastic leukemia cells with and
473 without ZFX knockout (19) (GEO GSE43020). These data revealed that genes
474 downregulated by ZFX knockout in mice have human homologs that are
475 specifically and significantly over-represented in Blue ($p=0.0005$) and Green
476 ($p=0.005$) modules ($p>0.1$ for each of the other 6 WGCNA modules) – providing
477 experimental validation of our hypothesized regulatory role for ZFX.
478
479
480
481
482

Figure 4 (next page). Weighted Gene Co-expression Network Analysis of Sex Chromosome Dosage Effects. a) Dot and line plots detailing mean expression (+/- 95% confidence intervals) by SCD group for 8 SCD-sensitive and functionally-coherent gene co-expression modules. **b)** Top 3 GO term enrichments for each module. **c)** Heatmap showing distinct profile of module DE with a supernumerary chromosome 21 vs. a supernumerary X-chromosome. **d)** Heatmap showing statistically significant differential expression of gene co-expression modules between karyotype groups. **e)** Cross tabulation showing enrichment of each module for the dosage-sensitive clusters of sex-chromosome genes detected by k-means. Lower-bounds for enrichment odds-ratios are given where mean enrichment = ∞. **f)** Gene co-expression network for the Blue module showing the top decile of co-expression relationships (edges) between the top decile of SCD-sensitive genes (nodes). Nodes are positioned in a circle for ease of visualization. Node shape distinguishes autosomal (circle) from sex chromosome (square) genes. Sex chromosome genes within the blue module are color coded by their SCD-sensitivity grouping as per **Figure 2a** (PAR-Orange, XCIE – dark green, XIST –purple). Larger node and gene name sizes reflect greater SCD sensitivity. Edge width indexes the strength of co-expression between gene pairs. **g).** ZFX and its target genes from Blue, Green and Brown modules with significant ZFX TFBS enrichment. Note that expression levels of ZFX (which increases in expression with mounting X-chromosome dosage) are positively correlated (solid edges) with SCD sensitive genes that are up-regulated by increasing X-chromosome dose (Blue and Green modules), but negatively correlated (dashed edges) with genes that are down-regulated by increasing X-chromosome dose (Brown module).

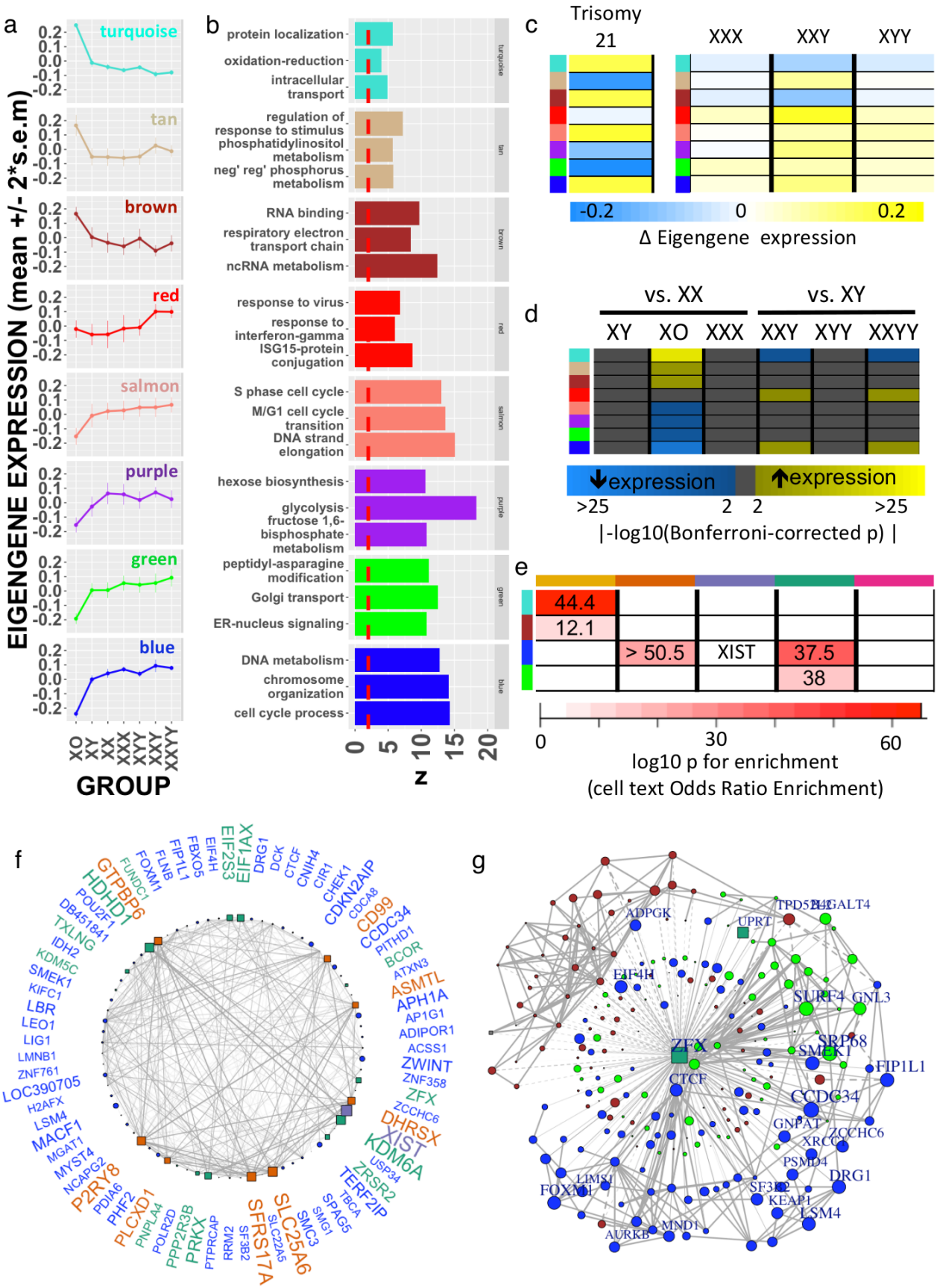
a
EIGENGENE EXPRESSION (mean +/- 2*s.e.m)
turquoise
tan
brown
red
salmon
purple
green
blue
XO XY XX XXX XYY XXY XXYY
GROUP
b
protein localization
oxidation-reduction
intracellular transport
regulation of response to stimulus
phosphatidylinositol metabolism
neg' reg' phosphorus metabolism
RNA binding
respiratory electron transport chain
ncRNA metabolism
response to virus
response to interferon-gamma
ISG15-protein conjugation
S phase cell cycle
M/G1 cell cycle transition
DNA strand elongation
hexose biosynthesis
glycolysis
fructose 1,6-bisphosphate metabolism
peptidyl-asparagine modification
Golgi transport
ER-nucleus signaling
DNA metabolism
chromosome organization
cell cycle process
z
c
Trisomy 21
XXX XXY XYY
-0.2 0 0.2
Δ Eigengene expression
d
vs. XX
vs. XY
XY XO XXX XXY XYY XXYY
expression
expression
>25 2 2 >25
|-log10(Bonferroni-corrected p) |
e
44.4
12.1
> 50.5
XIST
37.5
38
0 30 60
log10 p for enrichment
(cell text Odds Ratio Enrichment)
f
g
ADPGK
UPRT
EIF4H
SURF4
GNL3
ZFX
SRP68
SMEK1
FIP1L1
CTCF
CCDC34
GNPAT
ZCCHC6
XRCC1
PSMD4
DRG1
LIMS1
FOXM1
SF3B2
KEAP1
LSM4
AURKB
MND1

502

503 **DISCUSSION**

504 In conclusion, our study – which systematically examined gene expression
505 data from 470 individuals representing a total of 9 different sex chromosome
506 karyotypes - yields several new insights into sex chromosome biology with
507 consequences for basic and clinical science. First, our discovery and validation of
508 X-linked genes that are upregulated by reducing X-chromosome count – so that
509 their expression is elevated in XO vs. XX for example – runs counter to dominant
510 models of sex chromosome dosage compensation in mammals, and thereby
511 modifies current thinking regarding which subsets of X-chromosome genes could
512 contribute to sex and SCA-biased phenotypes (20). We speculate that this newly-
513 observed non-canonical mode of X-chromosome dosage sensitivity could arise
514 through one or more of the following candidate mechanisms: (i) repression of X-
515 linked genes on the active X-chromosome by genes that are expressed from
516 inactive X-chromosomes, and (ii) sensitivity of X-linked genes on the active X-
517 chromosome to the changes in nuclear heterochromatin dosage that would follow
518 from varying numbers of inactivated X-chromosomes (21).

519 Our findings also modify classical models of sex-chromosome biology by
520 identifying X-linked genes that vary in their expression as a function of Y–
521 chromosome dosage – indicating that the phenotypic effects of normative and
522 aneuploidic variations in Y-chromosome dose could theoretically be mediated by
523 altered expression of X-linked genes. Moreover, the discovery of Y chromosome
524 dosage effects on X-linked gene expression provides novel routes for
525 competition between maternally and paternally inherited genes beyond the

526 previously described mechanisms of parental imprinting and genomic conflict–
527 with consequences for our mechanistic understanding of sex-biased evolution
528 and disease (22).

529 Beyond their theoretical implications, our data help to pinpoint specific
530 genes that are likely to play key roles in mediating sex chromosome dosage
531 effects on wider genome function. Specifically, we establish that a distinctive
532 group of sex-linked genes - notable for their evolutionary preservation as X-Y
533 gametolog pairs across multiple species, and the breadth of their tissue
534 expression in humans (10) – are further distinguished from other sex-linked
535 genes by their exquisite sensitivity to SCD, and exceptionally close co-
536 expression with SCD-sensitive autosomal genes. These results add critical
537 evidence in support of the idea that X-Y gametologs play a key role in mediating
538 SCD effects on wider genome function. In convergent support of this idea we
539 show that (i) multiple SCD-sensitive modules of co-expressed autosomal genes
540 are enriched with TFBS for an X-linked TF from the highly dosage sensitive *ZFX-*
541 *ZFY* gemetolog pair, and (ii) ZFX deletion causes targeted gene expression
542 changes in such modules. Inclusion of ZFX in a co-expression module (Blue)
543 with enriched annotations for chromatin organization and cell cycle pathways is
544 especially striking given the rich bodies of experimental data which have
545 independently identified ZFX as a key regulator of cellular renewal and
546 maintenance (23).

547 Gene co-expression analysis also reveal the diverse domains of cellular
548 function that are sensitive to SCD – spanning cell cycle regulation, protein

549 trafficking and energy metabolism. These effects appear to be specific to shifts in
550 SCD as they are not induced by trisomy of chromosome 21. Furthermore, gene
551 co-expression analysis of SCD effects dissects out specific immune activation
552 pathways that are upregulated by supernumerary X-chromosomes in males, and
553 enriched for genes known to confer risk for autoimmune disorders that are
554 overrepresented amongst males bearing an extra X-chromosome. Thus, we
555 report coordinated genomic response to SCD that could potentially explain
556 observed patterns of disease risk in SCA.

557 Collectively, these novel insights serve to refine current models of sex-
558 chromosome biology, and advance our understanding of genomic pathways
559 through which sex chromosomes can shape phenotypic variation in health, and
560 sex chromosome aneuploidy.

561

562 **MATERIALS AND METHODS**

563

564 **Acquisition and preparation of biosamples**

565 RNA was extracted by standard methods (Qiagen, MD, USA) from
566 lymphoblastoid cell lines (LCLs) for 469 participants recruited through studies of
567 SCA at the National Institute of Health Intramural Research Program, and
568 Thomas Jefferson University (24). All participants with X/Y-aneuploidy were non-
569 mosaic, and stability of karyotype across LCL derivation was confirmed by
570 chromosome fluorescent in situ hybridization (FISH) in all members of a
571 randomly selected subset of 9 LCL samples representing each of the 4

572 supernumerary SCA groups included in our microarray analysis**.** Sixty-eight
573 participants provided RNA samples for microarray analyses (12 XO, 10 XX, 9
574 XXX, 10 XY, 8 XXY, 10 XYY, 9 XXYY), and 40 participants provided RNA
575 samples for a separate qPCR validation/extension study (4 XO, 145 XX, 22 XXX,
576 146 XY, 34 XXY, 16 XYY, 17 XXYY, 8 XXXY, 10 XXXXY). The microarray and
577 qPCR samples were fully independent of each other (biological replicates), with
578 the exception of 2 XO participants in the microarray study, who each also
579 provided a separate LCL sample for the qPCR study (**Table S1**).
580

581 **Microarray data preparation, differential expression analysis, annotation**
582 **and probe selection**

583 Gene expression was profiled using the Illumina HT-12 v4 Expression
584 BeadChip Kit (Illumina Inc, San Diego, CA). Expression data were quantile
585 normalized across arrays and log2 transformed using the *limma* package in
586 R(25). For each of 47323 probes, we estimated mean expression by karyotype
587 group, and log2 fold change in gene expression for each unique pairwise group
588 contrast between karyotype groups (**Fig. 1a**), along with their associated false-
589 discover-rate (FDR) corrected p-values. For each pairwise karyotype group
590 comparison, we identified probes with significant log2 fold-changes that survived
591 FDR correction for multiple comparisons across all 47323 probes with q (the
592 expected proportion of falsely rejected nulls) set at 0.05. We also calculated a
593 single summary estimate of SCD effects for each probe, by calculating the

594 proportion of variance (r^2) in probe expression that was accounted for by the 7-
595 level factor of SCD group.

596 All 47323 microarray probes were annotated using both the vendor
597 manifest file and an independently published re-annotation that assigns a quality
598 rating to each probe based on the specificity of its alignment to the purported
599 transcript target (26). We filtered for all probes with "perfect" or "good" quality
600 alignment to a known gene according to this reannotation, and then used the
601 *collapseRows* function from the WGCNA (27) package in R (with default
602 settings), to select one probe per gene. We also applied a further filter to remove
603 any Y-linked probes that showed differential expression between female
604 karyotype groups. These steps resulted in high-quality measures of expression
605 and estimates of differential expression for 19984 autosomal and 894 sex-
606 chromosome genes in each of 68 independent samples from 7 different
607 karyotype groups.

608 To select a log2 threshold for use in categorical definition of differentially
609 expressed genes (DEGs), we estimated DEG count across a range of absolute
610 log2 fold-change cut-offs for 6 contrasts of primary interest: karyotypically normal
611 males vs. females (i.e. XY vs. XX), and each SCA group vs. its respective
612 "gonadal control" (i.e XX was the control for XO and XXX groups / XY was the
613 control for XXY, XYY and XXYY). An absolute log2 fold change of 0.26
614 (equivalent to a ~20% increase/decrease in expression) was empirically selected
615 as the cut-off to define differential expression by (i) separately identifying the
616 increase in log2FC threshold that cause the greatest drop in DEG count for each

617 SCA group, (ii) averaging these log2FC thresholds across all 5 SCA groups.
618 Thus in any contrast between two karyotype groups, DEGs showed log 2 fold-
619 changes that met both of the following two criteria: an associated p value that
620 met FDR correction with q<0.05, and an absolute magnitude greater than 0.26.
621

622 **Identifying Genes Showing Significant Differential Expression Across All**
623 **Sampled Changes in X- and Y-Chromosome Count**

624 The 21 unique pairwise karyotype group comparisons in our microarray
625 dataset included 15 contrasts involving a disparity in X-chromosome count, and
626 16 contrasts involving a disparity in Y-chromosome count (**Fig. 1a**). Using the
627 empirically-defined |log2 fold change| cut-off of 0.26 (see above), we screened all
628 20878 genes for evidence of significant differential expression across all
629 instances of X- or Y-chromosome disparity.
630

631 **Comparing SCD Sensitivity of Gametolog vs. non-Gametolog Sex-Linked**
632 **Genes**

633 Fourteen of 16 established (9) X-Y gametolog gene pairs were
634 represented in our microarray dataset. To compare the SCD sensitivity of this
635 gene set to that of non-gametolog sex-linked genes we first quantified the mean
636 effect of SCD group on gene expression within the gametolog gene set by
637 averaging gene-wise r-squared values for the effect of SCD group on expression.
638 We then determined the centile of this observed gene set mean r-squared
639 against a distribution of r-squared values for 10,000 similarly sized sets of

640 randomly sampled non-gametolog sex-linked genes (**Fig. 1d**). This procedure
641 was conducted separately for X- and Y-chromosomes.
642
643 **A Priori Assignment of Sex Chromosome Genes to Four Class Model**
644 **Categories**
645 PAR genes were defined as those lying distal to the PAR1 and PAR2
646 boundaries specified in hg18 build of the human genome. Y-linked and X-linked
647 genes were defined as those lying proximal to these PAR boundaries on the Y-
648 and X-chromosome respectively. X-linked genes were assigned to XCIE and XCI
649 using consensus classifications from a systematic integration (8) of XCI calls
650 from 3 large-scale assays: expression from the inactivated human X-
651 chromosome in 9 hybrid human-mouse cell lines (12), allelic-imbalance analysis
652 of expression data in cell-lines from females with skewed X-inactivation (28), and
653 X-chromosome methylation data from microarray (29). According to the XCI
654 categories of this consensus report we classified X-linked genes as X-inactivated
655 ("Subject" or "Mostly Subject" categories), X-escape ("Escape" or "Mostly
656 Escape" categories), or X-other (all other intermediate categories).
657
658 **Clustering of Sex Chromosome Genes by Dosage Sensitivity**
659 For all 894 sex chromosome genes within our dataset we calculated the
660 mean fold-change per SCD group relative to mean expression across all SCD
661 groups. The resulting 894 by 7 matrix was submitted to k-means clustering
662 across a range of k-values using the *kmeans* function in R with nstart and

663 iter.max set at 100. Visual inspection of a scree plot of mean within partition sum-
664 of-squared residuals against k indicated an optimal 6-cluster solution (**Fig. S2a**).
665 The largest of these 6 clusters (Gray cluster) gathered genes with low or
666 undetectable expression levels across all samples, and was excluded from
667 further analysis.

668 Reproducibility of 6 cluster solution was established using a bootstrap
669 method whereby individuals were randomly drawn (with replacement) from each
670 SCD group within our microarray dataset to derive 1000 bootstrap sets of 68
671 samples. k-means clustering was repeated for each of these 1000 sets to define
672 a 6-cluster solution in each draw (**Fig. S2b**). Consistency of clustering was
673 quantified for each gene as the proportion of bootstrap draws in which it was
674 assigned to the same cluster as it had been in the original sample. The median
675 consistency score for cluster designation was >93% for all 5 clusters of SCD-
676 sensitive sex chromosome genes.

677 The observed grouping of sex chromosome genes from k-mean
678 clustering, was compared with the predicted Four Class Model groupings using
679 two-tailed Fishers tests for all pairwise cluster-grouping combinations (**Fig. 2b**).

680

681 **Modelling X- and Y-chromosome Dosage Effects on Expression of Sex**
682 **Chromosome Gene Clusters**

683 We used the following linear models to estimate the combined influence of
684 X and Y chromosome dosage in cluster and gene-level expression of Yellow
685 (XCI enriched) and Green (XCIE enriched) gene clusters:

686 Expression ~ β_0 (intercept) + β_1(X_count) + β_2(Y_count) + error

687 We computed p-values for comparisons of both β_1 and β_2 coefficient
688 estimates against the null (0), and used these to test for significant directional
689 effects of sex chromosome dosage on the mean expression of each gene
690 cluster, as well the expression of individual genes within each cluster.

691

692 **Aligning Sex Chromosome Expression, Epigenetic and Evolutionary Data**

693 We validated our data-driven clustering of X-linked genes into Yellow (XCI
694 enriched) and Green (XCIE enriched) groups, by overlapping the genomic
695 coordinates of gene probes with segmentations of the X-chromosome according
696 to (i) "chromatin states" defined by computational analysis of coordinated
697 changes in 10 distinct chromatin marks in LCLs (16), (ii) "evolutionary strata"
698 reflecting staged loss of recombination between the X- and Y-chromosome (15).
699 Overlaps of our probe coordinate with these two annotations were defined using
700 the GenomicRanges package in R. As a third validation we also aligned our
701 clustering of X-lined genes with a previously published annotation of X-linked
702 genes according to whether their corresponding ancestral Y-linked homologue
703 has been lost, converted to a pseudogene or maintained (8). Non-random
704 associations between these three annotations and Yellow vs. Green k-means
705 cluster membership were assessed using Chi-squared tests.

706

707

708

709 **Comparison of DEG Count and Genomic Distribution Across SCA Groups**

710 Total DEG counts were compared across SCD groups across a range of
711 log 2 fold change cut-offs as described above and reported in **Fig. 3 a,b**. To test
712 for non-random distribution of DEGs across the genome in each SCD group **(Fig.**
713 **3c**), we compared observed DEG counts across 4 genomic regions - autosomal,
714 PAR, Y-linked and X-linked - to the background distribution of total gene counts
715 across these regions using the prop.test function in R. All SCD groups showed a
716 high non-random distribution of DEGs across the genome – reflecting preferential
717 involvement of sex chromosome genes ($p < 7.2 * 10^{-13}$).

718

719 **Quantitative rtPCR validation of Differentially-Expressed Genes in**
720 **Microarray**

721 *Selecting genes of interest:* For selected genes showing significant differential
722 expression between karyotype groups in our core sample, we used qPCR to
723 validate and extent observed fold-changes in an independent sample of 402
724 participants representing all the karyotypes in our core sample plus two
725 additional SCAs: XXXY, and XXXXY. Selection of specific genes for qPCR
726 validation was as follows. From the set of 10 sex-linked genes with patterns of
727 "obligate" dosage sensitivity (**Fig 1b**), we selected XIST, the 2 most X-
728 chromosome sensitive X-linked gametologs [EIF1AX, KDM6A(UTX)], and the 2
729 most Y-chromosome sensitive Y-linked gametologs (ZFY, DDX3Y). All genes
730 selected for qPCR from the sets of dosage sensitive sex chromosome genes
731 defined by k-means clustering (**Fig. 2a,b**) showed (i) stable cluster membership

732 in >95% of bootstrap draws (**Fig. S2b**), and (ii) consistent inclusion in the top 10
733 DEGs across multiple relevant group contrasts for that k-means cluster (Pink Y-
734 linked cluster: XYY vs. XY and XXYY vs. XXY | Yellow XCI and Green XCIE
735 clusters: XO vs. XXX, XO vs. XY, XXY vs. XX).
736 *Fluidigm qPCR protocol:* Reverse Transcription reaction was performed using
737 RT2 HT First Strand Kit (QIAGEN, 330411) with 1000 ng RNA input per sample.
738 One-tenth of cDNA was preamplified using RT2 Microfluidics qPCR Reagent
739 system (QIAGEN, 330431) in combination with custom RT2 PreAmp pathway
740 primer mix Format containing 94 RT2 primer assays. Fourteen cycles of
741 preamplification were performed using the manufacturer recommended
742 preamplification protocol. Amplified cDNA was diluted 5-fold using RNase-free
743 water and assessed in real-time PCR using the RT2 Micrifluidics EvaGreen
744 qPCR Master mix and a Custom RT2 profiler PCR array PCR Array containing
745 96 assays, including selected DEGs of interest, housekeeping genes, reverse-
746 transcription controls, and positive PCR control. Real-time PCR was performed
747 on a Fluidigm BioMark HD (Fluidigm, San Francisco, US) using the RT2 cycling
748 program for the Fluidigm BioMark, which consists of an initial thermal mix stage
749 (50°C for 2 minutes, 70°C for 30 minutes, and 25°C for 10 minutes) followed by a
750 hot start at 95°C for 10 minutes and 40 cycles of 94°C for 15 seconds, and 60°C
751 for 60 seconds. For data processing, an assay with Ct > 23 was deemed to be
752 not expressed.
753 *Differential Expression Analysis of qPCR data*: The ΔΔCT method of relative
754 quantification was used to analyze qPCR data (30). To provide normalized

755 estimates of expression for each gene we calculated ΔCT values, by subtracting
756 the CT for each gene of interest from the mean CT of two housekeeping genes
757 (GAPDH and RPLP0) which were not differentially expressed across groups in
758 either microarray or qPCR data. Thus, larger ΔCT values reflected greater
759 normalized expression relative to mean expression of the reference
760 housekeeping genes. These ΔCT values were used as input for calculation of all
761 unique pairwise group differences in expression between karyotype groups
762 represented in the independent qPCR validation dataset. Group differences in
763 expression were modeled using the limma R package with identical setting to
764 those used in analysis of microarray data (see above). The resulting ΔΔCT
765 represent fold-changes in gene expression between groups, on a log scale with a
766 base determined by the effective qPCR efficiency.

767 *Validation Microarray Results Using qPCR Results:* All 21 unique pairwise SCD
768 group contrasts in our microarray sample could be reproduced in the
769 independent qPCR dataset. We used the correlation across these 21 group
770 contrasts for the qPCR fold-change and microarray log2 fold change to quantify
771 the degree of agreement between qPCR and microarray findings (**Fig. S1a and**
772 **Fig. S2d,e**).

773 *Extension of Microarray Results Using qPCR Results:* The qPCR dataset also
774 included two SCD groups that were not represented in the microarray dataset –
775 XXXY and XXXXY – allowing for a total of 15 novel pairwise SCD group
776 contrasts ("XO-XXXY", "XO-XXXXY", "XXXY-XX", "XXXXY-XX", "XXX-XXXY", "XXX-
777 XXXXY", "XXXY-XY", "XXXXY-XY", "XXY-XXXY", "XXY-XXXXY", "XYY-XXXY", "XYY-
778 XXXXY", "XXYY-XXXY", "XXYY-XXXXY", "XXXY-XXXXY") sampling diverse disparities of

779 X- and Y-chromosome dosage. These novel contrasts were used as a further
780 test for the validity and reproducibility of our microarray findings. Each of the 15
781 novel pairwise SCD group contrasts was coded according to two effects of
782 interest: difference in X-chromosome count and difference in Y-chromosome
783 count. These coded SCD disparities were then correlated with observed fold-
784 changes for unique pairwise group contrasts in the qPCR dataset to test if
785 patterns of fold-change observed in the microarray dataset could be extension
786 into unseen karyotype groups (**Fig. S1b**,**c**: X- and Y-linked genes with
787 "obligatory" sex chromosome dosage sensitivity | **Fig. S2f,g**: X-linked genes from
788 the "Yellow" and "Green" k-means that countered expectations of the classical
789 Four Class Model).
790

791 **Weighted Gene Co-expression Network Analysis (WGCNA)**

792 *Defining Gene Co-expression Modules*: Gene co-expression modules were
793 generated using the R package Weighted Gene Co-expression Network Analysis
794 (WGCNA). Briefly, this involved first calculating the Pearson correlation
795 coefficient between all 20978 genes across all 68 samples in our study. This
796 correlation matrix was transformed using a signed power adjacency function with
797 a threshold power of 12 (selected based on fit to scale-free topology), and then
798 converted into Topological Overlap Matrix (TOM) by modifying the correlation
799 between each pair of genes using a measure of the similarity in their respective
800 correlations with all other genes (31). The resulting TOM was then converted to a
801 distance matrix by subtraction from 1, and used to generate a dendrogram for

802 clustering genes into modules. Gene modules were defined using the Dynamic
803 Hybrid cutree function (32) [with the following parameter settings: deepSplit
804 (control over sensitivity of module detection to module splitting) = 2,
805 mergeCutHeight (distance below which modules are merged)= 0.25, minimum
806 module size=30)]. Given the large number of genes included in our analyses, we
807 implemented module detection using the "blockwise" WGCNA algorithm, which
808 starts with a computationally inexpensive method to assort genes into smaller co-
809 expression blocks, and then completes the above steps within each block before
810 merging module designations across blocks. This implementation of WGCNA
811 defined 18 mutually exclusive co-expression gene modules within our data,
812 which ranged from 45 to 1393 genes in size, and a left-over group of 14630
813 genes without module membership (**Table S3**). The expression of each module
814 was summarized as a module eigengene value (ME: the right singular vector of
815 standardized expression values for genes in that module) in every sample. These
816 ME values were used to determine differential expression of modules across
817 (omnibus F-tests) and between (T-tests) SCD groups, as well as module co-
818 expression across samples (Pearson correlation coefficient).
819 *Further characterizing gene co-expression modules*: We used module
820 preservation analysis to establish that our defined co-expression modules were
821 not dominated by (i) the large number of DEGs induced by X-monosomy (using
822 expression data excluding XO samples), or (ii) other SCD group differences in
823 mean expression levels (using expression data after residualization for the
824 effects of SCD group and re-centering at a common mean). All modules showed

825 high reproducibility based on a module-specific $Z_{summary}$ scores derived by
826 comparing observed modular connectivity and density metrics with null values
827 generated by 200 permutations of gene-level module membership(33). We
828 focused further characterization of modules which passed two independent
829 statistical criteria; (i) SCD sensitivity - quantified using F-tests for the omnibus
830 effects of karyotype group on modular expression quantified as the ME, (ii)
831 functional coherence as inferred by analysis of modular gene ontolology term
832 enrichments using GO elite (34), and Gorilla (35).
833 *Testing for enrichment of autoimmune disorder risk genes in WGCNA modules:*
834 A large-scale records-based study was used to define 10 Autoimmune Disorder
835 (ADs) with clearly elevated prevalence rates in XXY vs. XY males (7), 9 of which
836 were represented in the largest available catalog of Genome Wide Association
837 Study (GWAS) findings (https://www.ebi.ac.uk/gwas/): Diabetes Mellitus type 1,
838 Multiple Sclerosis, Autoimmune Hypothyroidism, Psoriasis, Rheumatoid Arthritis,
839 Sjogren's Syndrome, Systemic Lupus Erythematosus, Ulcerative Colitis, and
840 Coeliac Disease. A total of 495 genes within our microarray sample were
841 annotated for showing a significant association in GWAS with one or more of
842 these 9 AD conditions. Overrepresentation of this AD gene set in the XXY
843 upregulated Red gene co-expression module was tested for using both Fisher's
844 exact test (p=0.01), and by comparing the observed representation of AD genes
845 against a null distribution generated by 10,000 random gene samples of equal
846 size to the red module.

847 *Testing for patterned enrichment of dosage sensitive sex chromosome genes in*
848 *WGCNA modules:* We tested if any of the 8 SCD-sensitive and functionally
849 enriched WGCNA modules showed enrichment for the previously derived k-
850 means clusters of dosage sensitive sex chromosome genes (**Fig. 2**) by applying
851 two-tailed Fishers tests to all pairwise module-cluster combinations (**Fig. 4 e**). All
852 observed associations survived Bonferroni correction for multiple comparisons.
853 *Module Visualization:* WGCNA co-expression modules were visualized by
854 selecting genes within the top decile of SCD-sensitivity (indexed using r-squared
855 for proportion of expression variance explained by group), and edges (co-
856 expression links between genes) in the top decile of edge strengths. All
857 visualizations were constructed using the igraph R package in R.
858 *Transcription factor binding site analyses:* Transcription factor binding site
859 (TFBS) enrichment analysis was performed each of the 4 SCD-sensitive
860 WGCNA modules - Blue, Green, Turquoise and Brown - that were enriched for
861 inclusion of gene from one or more of the 5 SCD-sensitive clusters of sex
862 chromosome genes. In each module, we scanned canonical promoter regions
863 (1000bp upstream of the transcription start site) for the top 500 genes with
864 strongest intramodular "connectivity" (based on kME - the magnitude of each
865 gene's coexpression with its module's eigengene). Next we utilized TFBS
866 position weight matrices (PWMs) from JASPAR database (205 non-redundant
867 and experimentally defined motifs) (36) to examine the enrichment for
868 corresponding TFBS within each module. For TFBS enrichment all the modules
869 were scanned with each PWMs using the Clover algorithm (37). To compute the

870 enrichment analysis, we utilized three different background datasets (1000 bp
871 sequences upstream of all human genes, human CpG islands and human
872 chromosome 20 sequence). To increase confidence in the enrichment analyses,
873 we considered TFBS to be over-represented based on the P-values (<0.05)
874 obtained relative to all the three corresponding background datasets.
875 *Enrichment of SCD sensitive modules for genes with DE due to experimental*
876 *ZFX knockout.* To provide an orthogonal experimental test for evidence of a
877 regulatory role for ZFX within Blue, Green or Brown WGCNA modules, we used
878 a list of genes with significantly decreased expression due to ZFX knockout in
879 murine lymphocytes(19). Human homologs were found for these genes
880 (http://www.informatics.jax.org/downloads/reports/index.html), and two-tailed
881 Fishers Tests were used to assess if these human genes were significantly
882 enriched/impoverished in any of the 8 SCD sensitive WGCNA modules.
883
884 **Comparison of Autosomal Gene Fold-Change in SCA and Down Syndrome**
885 The transcriptomic effects on Trisomy 21 (T21) were characterized in
886 LCLs by passing a publically available Illumina microarray gene expression
887 dataset (GEO, Accession number GSE34458) through an identical analytic
888 pipeline to that used in characterizing genome-wide fold changes in our SCA
889 sample (see above). We first independently confirmed the previously reported
890 finding that chromosome 21 was robustly enriched for genes showing differential
891 expression in this T21 data set (Chi-squared=999, p<2*10-16 for enrichment of
892 DEGs on chromosome 21) – buttressing use of these data to assess

893 transcriptomic effects of T21. We examined overlaps in genome-wide expression
894 change between T21 and the three sex-chromosome trisomes in our samples
895 (XXY, XYY and XXX) using 17671 genes with complete expression data in both
896 microarray datasets (after exclusion of genes on chromosomes X, Y and 21).
897 We tested for, and failed to find any evidence of significant overlap in DEGs
898 using Chi-squared tests (**Table S4**). To test if T21 showed a similar shift in gene
899 co-expression modules to sex chromosome trisomies, we used the designation
900 of genes to modules in the SCA sample to recalculate module Eigengenes. We
901 then calculated MR fold changes for T21 and three SCA trisomies (XXX, XXY
902 and XYY). Trisomy of chromosome 21 was associated with a clearly distinct
903 profile of ME expression chance than all three of the SCA trisomies (**Fig. 4c**).

REFERENCES

1. Hughes JF, Rozen S (2012) Genomics and genetics of human and primate y chromosomes. *Annu Rev Genomics Hum Genet* 13:83–108.

2. Arnold AP (2012) The end of gonad-centric sex determination in mammals. *Trends Genet* 28(2):55–61.

3. Bermejo-Alvarez P, Rizos D, Rath D, Lonergan P, Gutierrez-Adan A (2010) Sex determines the expression level of one third of the actively expressed genes in bovine blastocysts. *Proc Natl Acad Sci U S A* 107(8):3394–3399.

4. Petropoulos S, et al. (2016) Single-Cell RNA-Seq Reveals Lineage and X Chromosome Dynamics in Human Preimplantation Embryos. *Cell* 165(4):1012–1026.

5. Belling K, et al. (2017) Klinefelter syndrome comorbidities linked to increased X chromosome gene dosage and altered protein interactome activity. *Hum Mol Genet* 26(7):1219–1229.

6. Hong DS, Reiss AL (2014) Cognitive and neurological aspects of sex chromosome aneuploidies. *Lancet Neurol* 13(3):306–318.

7. Seminog OO, Seminog AB, Yeates D, Goldacre MJ (2015) Associations between Klinefelter's syndrome and autoimmune diseases: English national record linkage studies. *Autoimmunity* 48(2):125–128.

8. Balaton BP, Cotton AM, Brown CJ (2015) Derivation of consensus inactivation status for X-linked genes from genome-wide studies. *Biol Sex Differ* 6:35.

9. Skaletsky H, et al. (2003) The male-specific region of the human Y chromosome is a mosaic of discrete sequence classes. *Nature* 423(6942):825–37.

10. Bellott DW, et al. (2014) Mammalian Y chromosomes retain widely expressed dosage-sensitive regulators. *Nature* 508(7497):494–499.

11. Deng X, Berletch JB, Nguyen DK, Disteche CM (2014) X chromosome regulation: diverse patterns in development, tissues and disease. *Nat Rev Genet* 15(6):367–378.

12. Carrel L, Willard HF (2005) X-inactivation profile reveals extensive variability in X-linked gene expression in females. *Nature* 434(7031):400–4.

13. Tukiainen T, et al. (2017) Landscape of X chromosome inactivation across human tissues. *Nature* 550(7675):244–248.

14. Wilson Sayres MA, Makova KD (2013) Gene survival and death on the human Y chromosome. *Mol Biol Evol* 30(4):781–787.

15. Pandey RS, Wilson Sayres MA, Azad RK (2013) Detecting evolutionary strata on the human x chromosome in the absence of gametologous y-linked sequences. *Genome Biol Evol* 5(10):1863–1871.

16. Ernst J, et al. (2011) Mapping and analysis of chromatin state dynamics in nine human cell types. *Nature* 473(7345):43–49.

17. Aksglaede L, Juul A (2013) Testicular function and fertility in men with Klinefelter syndrome: a review. *Eur J Endocrinol Eur Fed Endocr Soc* 168(4):R67-76.

18. Parikshak NN, Gandal MJ, Geschwind DH (2015) Systems biology and gene networks in neurodevelopmental and neurodegenerative disorders. *Nat Rev Genet* 16(8):441–458.

19. Weisberg SP, et al. (2014) ZFX controls propagation and prevents differentiation of acute T-lymphoblastic and myeloid leukemia. *Cell Rep* 6(3):528–540.

20. Disteche CM (2016) Dosage compensation of the sex chromosomes and autosomes. *Semin Cell Dev Biol* 56:9–18.

21. Wijchers PJ, Festenstein RJ (2011) Epigenetic regulation of autosomal gene expression by sex chromosomes. *Trends Genet TIG* 27(4):132–140.

22. Cocquet J, et al. (2012) A genetic basis for a postmeiotic x versus y chromosome intragenomic conflict in the mouse. *PLoS Genet* 8(9):e1002900.

23. Galan-Caridad JM, et al. (2007) Zfx controls the self-renewal of embryonic and hematopoietic stem cells. *Cell* 129(2):345–357.

24. Zinn AR, et al. (2007) A Turner syndrome neurocognitive phenotype maps to Xp22.3. *Behav Brain Funct BBF* 3:24.

25. Ritchie ME, et al. (2015) limma powers differential expression analyses for RNA-sequencing and microarray studies. *Nucleic Acids Res* 43(7):e47.

26. Barbosa-Morais NL, et al. (2010) A re-annotation pipeline for Illumina BeadArrays: improving the interpretation of gene expression data. *Nucleic Acids Res* 38(3):e17.

27. Langfelder P, Horvath S (2008) WGCNA: an R package for weighted correlation network analysis. *BMC Bioinformatics* 9:559.

28. Cotton AM, et al. (2013) Analysis of expressed SNPs identifies variable extents of expression from the human inactive X chromosome. *Genome Biol* 14(11):R122.

29. Cotton AM, et al. (2015) Landscape of DNA methylation on the X chromosome reflects CpG density, functional chromatin state and X-chromosome inactivation. *Hum Mol Genet* 24(6):1528–1539.

30. Schmittgen TD, Livak KJ (2008) Analyzing real-time PCR data by the comparative C(T) method. *Nat Protoc* 3(6):1101–1108.

31. Zhang B, Horvath S (2005) A general framework for weighted gene co-expression network analysis. *Stat Appl Genet Mol Biol* 4:Article17.

32. Langfelder P, Zhang B, Horvath S (2008) Defining clusters from a hierarchical cluster tree: the Dynamic Tree Cut package for R. *Bioinforma Oxf Engl* 24(5):719–720.

33. Langfelder P, Luo R, Oldham MC, Horvath S (2011) Is my network module preserved and reproducible? *PLoS Comput Biol* 7(1):e1001057.

34. Zambon AC, et al. (2012) GO-Elite: a flexible solution for pathway and ontology over-representation. *Bioinforma Oxf Engl* 28(16):2209–2210.

35. Eden E, Navon R, Steinfeld I, Lipson D, Yakhini Z (2009) GOrilla: a tool for discovery and visualization of enriched GO terms in ranked gene lists. *BMC Bioinformatics* 10:48.

36. Portales-Casamar E, et al. (2010) JASPAR 2010: the greatly expanded open-access database of transcription factor binding profiles. *Nucleic Acids Res* 38(Database issue):D105-110.

37. Frith MC, et al. (2004) Detection of functional DNA motifs via statistical over-representation. *Nucleic Acids Res* 32(4):1372–1381.